CrystEngComm

Accepted Manuscript

This is an *Accepted Manuscript*, which has been through the Royal Society of Chemistry peer review process and has been accepted for publication.

Accepted Manuscripts are published online shortly after acceptance, before technical editing, formatting and proof reading. Using this free service, authors can make their results available to the community, in citable form, before we publish the edited article. We will replace this *Accepted Manuscript* with the edited and formatted *Advance Article* as soon as it is available.

You can find more information about *Accepted Manuscripts* in the Information for Authors.

Please note that technical editing may introduce minor changes to the text and/or graphics, which may alter content. The journal's standard Terms & Conditions and the Ethical guidelines still apply. In no event shall the Royal Society of Chemistry be held responsible for any errors or omissions in this *Accepted Manuscript* or any consequences arising from the use of any information it contains.

ROYAL SOCIETY OF CHEMISTRY

www.rsc.org/crystengcomm

CrystEngComm RSCPublishing

ARTICLE

The growth and assembling of the multidimensional hierarchical Ni_3S_2 for aqueous asymmetric supercapacitors

Cite this: DOI: 10.1039/x0xx00000x

Bin Yang,[a] Lei Yu,[a] Qi Liu,[a] Jingyuan Liu,*[a] Wanlu Yang,[a] Hongsen Zhang,[a] Feihong Wang,[a] Songxia Hu,[b] Yi Yuan,[a] Jun Wang*[ab]

Received 00th January 2012,
Accepted 00th January 2012

DOI: 10.1039/x0xx00000x

www.rsc.org/

The mushroom-like Ni_3S_2 consisting of thin film on the nanorods arrays has been successfully synthesized by a dissolution-precipitation route, which carried out by a hydrothermal process using the Ni foam in the thioacetamide alcohol solution without the introduction of other Ni sources. The thin film played a key role in exhibiting an excellent electrochemistry performance for the mushroom-like Ni_3S_2 electrode. As pseudocapacitor materials, the as-obtained mushroom-like Ni_3S_2 electrode showed a significantly specific capacitance (1190.4 F g^{-1} at 8 A g^{-1}). Moreover, the asymmetric supercapacitor, with the mushroom-like Ni_3S_2 as the positive electrode material and the active carbon powder (AC) as the negative electrode material, exhibited a high energy density (60.3 W h kg^{-1}) at an average power density of 3600 W kg^{-1} based on the mass of active material.

1. Introduction

Supercapacitors have been demonstrated as a promising energy storage device, because of high power performance, long life cycle and low maintenance cost, but the low energy density is a mainly problem to restrict the practical applications.[1-4] According to the equation (1) to calculate energy density:

$$E=\frac{1}{2}CV^2 \quad (1)$$

The improvement of energy density (E) can be achieved by maximizing the specific capacitance (C) and/or the cell voltage (V). Some reports exhibit that the organic electrolyte increases the voltage window (up to 3-3.5V), but the poor ion transfer rate, high cost and toxic nature limit the practical application.[5-7] Compared with the symmetric supercapacitors, the asymmetric supercapacitors have been demonstrated an effectively promising strategy to increase the energy density, due to these asymmetric supercapacitors consist of a battery-type Faradaic electrode (as the energy source) and a capacitor-type electrode (as the power source).[8,9] Therefore, the aqueous asymmetric supercapacitors which can make full use of the different potential windows of the two electrodes to supply a maximum voltage window (up to 1.6-2.0V) exhibit not only a higher energy density, but also a power density.[10]

However, the selection of electrode materials is an even more significant factor to determine performance of the supercapacitors. Compared with the electrical double-layer capacitor materials, the pseudocapacitor materials, including Co_3O_4 [11-13], layered double hydroxide (LDH)[14,15], $Ni(OH)_2$ [16] and $NiCo_2O_4$ [17-19], possess higher specific capacitance and energy density, due to interfacial reversible faradaic reaction to store energy. However, they usually suffer from poor electrical conductivity, poor ion transport kinetics, pronounced volume expansion and contraction during the charge-discharge processes.[20,21]

It is noted that the pseudocapacitive materials which grow on the conductive substrates have been investigated for emerging binder and conductive-free energy storage devices.[18,22] It solves the problem that the conductive agent and a polymer binder seriously limit the electrochemistry performance of the traditional electrode materials. More significantly, the pseudocapacitor materials which grow on the conductive substrates exhibit some advantages, including rich accessible electroactive sites, sufficient electrochemical reaction of the surface of materials and good electroactive contact with substrates.[23-25] For further obtaining the satisfactory electrochemistry performance, synthesis of the nanostructure materials is an effective strategy. Compared with the traditional materials of electrode, the nanostructure materials provide a promising solution to improve the specific capacitance and energy density because of high specific surface area, short electron and ion transport pathways.[3,26-28] However, the nanostructure materials easily self-aggregate due to the high specific surface energy, indicating that this issue decreases the specific surface area and adequately uses of entire nanostructure materials, resulting in a less satisfactory practical capacitance.[29] The advanced nanostructure is designed to prevent the nanostructure self-

CrystEngComm Accepted Manuscript

aggregation. To solve the above-mentioned problem, synthesis of nanostructured mesoporous materials, including nanoparticles, nanosheets, hollow-nanoarchitectures and one-dimensional (1D) nano-structure grow on the conductivity substrates has been proven to be an effective strategy.[27,30]

Recently, transition metal sulfides (such as NiS,[31] Ni_3S_2 [32-38] and $NiCo_2S_4$ [39,40]) have drawn great interest for electrochemical energy storage applications due to the satisfactory redox reaction of their metal ion. For example, yang *et al*. reports that the hierarchical flower-like-NiS prepared from solvothermal method exhibits a high specific capacitance of 857.76 F g^{-1} at 2 A g^{-1}.[41] Dai *et al*. fabricated the Ni_3S_2/carbon nanotube composites by hydrothermal method and the specific capacitance is 800 F g^{-1} at 2 A g^{-1} current densitsy. In the two-system electrochemistry measurement, a high performance asymmetric supercapacitor was successfully fabricated by using Ni_3S_2/CNT as the positive electrode and active carbon (AC) as the negative electrode, which exhibits an high energy density (19.8 W h kg^{-1} at 798 W kg^{-1}).[42] Chen *et al*. synthesized the $NiCo_2S_4$ nanotube arrays on the Ni foam, and the $NiCo_2S_4$ electrode exhibited a high areal capacitance (4.68 F cm^{-2} at 10 mA cm^{-2}), high energy density (31.5 Wh kg^{-1} at 156.6 W kg^{-1}) and high power density (2348.5 W kg^{-1} at 16.6 Wh kg^{-1}) can be achieved by assembling asymmetric supercapacitor with reduced graphene oxide at a total active material mass loading as high as 49.5 mg.[43] Therefore, it will be of great significance to develop a simple and facile way to synthesis the transition metal sulfides on the conductive substrates with advanced nanostructures.

In this report, we present a simple one-step dissolution-precipitation route for the in-situ growth of the mushroom-like Ni_3S_2 on the Ni foam. It only involves a simple hydrothermal process using the Ni foam in the thioacetamide (TAA) alcohol solution without the introduction of other Ni sources, surfactant and template. The nanorods Ni_3S_2 arrays were prepared with a reaction time of 12 h and the mushroom-like Ni_3S_2 was obtained after reaction time of 24 h. Compared with the nanorods Ni_3S_2 arrays electrode, the mushroom-like Ni_3S_2 presented rich accessible electroactive sites and superior electron collection efficiency at the electrochemistry performance measurement.[29] Accordingly, the thin film solved the serious problem that the nanorods Ni_3S_2 arrays have a fast fading of capacitance for the mushroom-like Ni_3S_2 electrode.[44] At the same time, the mushroom-like Ni_3S_2 electrode shows an excellent electrochemistry performance. The areal specific capacitance of the mushroom-like Ni_3S_2 electrode is 3.3 F cm^{-2} and the capacitance remains 86.9% of initial capacitance after 5000 cycles at the current density of 4 A g^{-1}. The asymmetric supercapacitor which is made up of the mushroom-like Ni_3S_2 arrays (positive electrode) and active carbon (negative electrode) exhibited the specific energy density of 60.3 W h kg^{-1} and specific power density of 3600 W kg^{-1}. And after 5000 cycles, the specific capacitance remained 80.2% of the initial capacitance.

2. Experimental

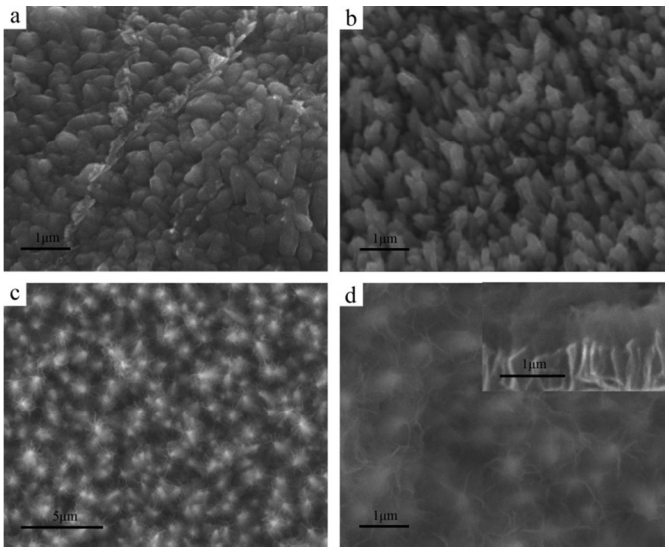

Fig. 1 SEM images of Ni_3S_2 in difference morphologies Ni_3S_2 (a) nanobulges, (b) nanorods, (c) and (d) mushroom-like Ni_3S_2

Fabrication of the mushroom-like Ni_3S_2 and nanorods Ni_3S_2 electrodes:

Typically, nickel foams (30×25×1.5mm) were pretreated with 3M HCl solution, deionized water, acetone or ethanol by ultrasonic washing 15 min, respectively. The 30 mg TAA was dissolved in 35 mL ethanol and then transferred into a 50 mL Teflon-lined stainless steel autoclave. After that, the cleaned Ni foam was immersed into reaction solution and maintained at 160 ^oC. The nanorods Ni_3S_2 arrays were obtained after 12 h, and the mushroom-like Ni_3S_2 was fabricated after 24 h. After reaction, the Ni foam was washed with deionized water and ethanol to remove surfaces ion and vacuum dried in 60 ^oC for 24h. The weight of mushroom-like Ni_3S_2 and nanorods Ni_3S_2 arrays are 2.51 and 2 mg. cm^{-2} on the Ni foam.

Fabrication of the Active carbon (AC) electrode:

First, the commercial (active carbon) AC, acetylene black and polyvinylidenedifluoride (PVDF) at ratio of 85:10:5 were uniformly dispersed in alcohol. And then the homogeneous paste was pressed onto Ni Foam (2×1 cm^2). Finally, the fabricated electrode was dried under vacuum at 60 ^oC for 1 day.

Characterization:

The morphologies of the products were observed by scanning electron microscope (SEM; JEOL JSM-6480A microscope, Tokyo, Japan) and transmission electron microscope (TEM; FEI company Tecnai G2 20 S-twin, 200kV). The crystalline structure was characterized by X-ray-diffraction system (XRD, Rigaku TTR-III) equipped with Cu Kα radiation (λ=0.15406nm)

Electrochemistry measurement:

CrystEngComm Accepted Manuscript

This journal is © The Royal Society of Chemistry 2012

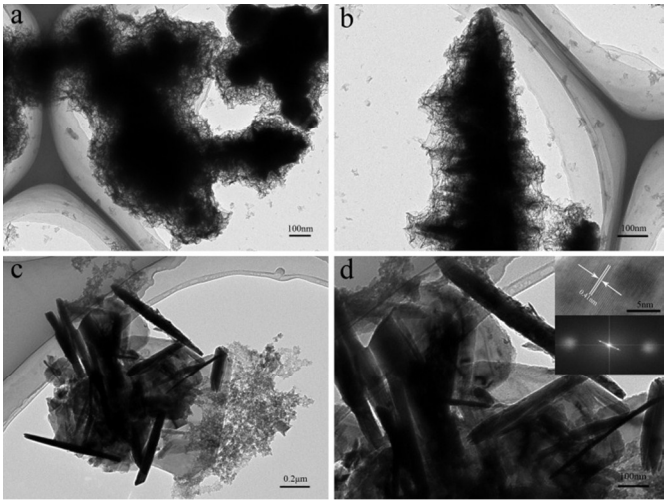

Fig. 2 (a) TEM image of nanobulges Ni_3S_2 (b) TEM image of nanorods Ni_3S_2 (c) TEM image of mushroom-like Ni_3S_2 (d) TEM, HRTEM, the corresponding FFT pattern images of mushroom-like Ni_3S_2.

The electrochemistry performance measurement of the mushroom-like Ni_3S_2, nanorods Ni_3S_2 arrays and AC electrode was investigated under a three-electrode cell with 2 M KOH electrolyte at 25 ^oC. The mushroom-like Ni_3S_2, nanorods Ni_3S_2 arrays and AC electrode were acted directly as working elec trodes. The saturated calomel electrode and Pt foil were acted as reference electrode and counter electrode, respectively.

The asymmetric supercapacitor is assembled by the mushroom-like Ni_3S_2 on the Ni foam as positive electrode and AC as negative electrode with 6M KOH electrolyte. The quality ratio of positive and negative electrode was calculated by charge balance theory ($q_+=q_-$). And the charge stored (q) by each electrode was calculated for the following equation (2):

$$q=C\times\Delta V\times m \quad (2)$$

Where C (F g^{-1}) is the specific capacitance of the electrode, ΔV (V) is the potential window from the galvanostatic charge-discharge for the electrode. All of the above measurements were conducted on a CHI 660D electrochemical workstation (ShangHai CH Instrument Company, China).

3. Results and discussion

Fig. 1 shows the SEM images of Ni_3S_2 after the reaction time of 6 h, 12 h and 24 h. As shown in Fig. 1a, Ni_3S_2 nanobulges were preserved after 6 h in the hydrothermal reaction. With the reaction time increasing to 12 h, the nanorods Ni_3S_2 arrays were obtained, as shown in Fig. 1b. After 24 h, the thin film grew on the top of nanorods arrays to form the mushroom-like Ni_3S_2 is presented in Fig.1c and d. Fig. 1c exhibits the mushroom-like Ni_3S_2 uniformly grew on the Ni foam. The high magnification SEM image (Fig. 1d) demonstrates the mushroom-like structure and several nanofolds around nanorods Ni_3S_2 arrays obviously. The inset in Fig. 1d is a sectional view of the mushroom-like structure and clearly exhibits the mushroom-like structure which is a mass of nanosheets aggregation to form the thin film on the nanorods arrays.

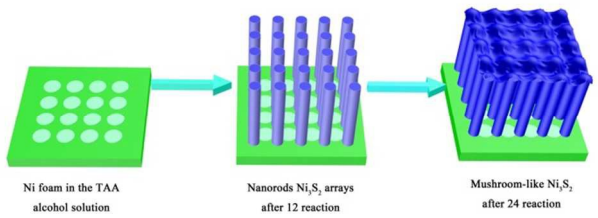

Fig. 3 Schematic illustration of synthetic mushroom-like Ni_3S_2 on the Ni foam.

From the TEM images of Fig. 2a and b, a mass of ultrathin nanosheets uniformly coat on the surface of the nanobulges and nanorods Ni_3S_2. However, the TEM images of the mushroom-like Ni_3S_2 (Fig. 2c and d) are different from Ni_3S_2 nanobulges and nanorods. The thin film and nanorods Ni_3S_2 are observed from the Fig. 2c and d, because the overall structure of the mushroom-like Ni_3S_2 was destroyed by preparing the sample. Besides, the ultrathin nanosheets are observed from the TEM image of the mushroom-like Ni_3S_2 due to several nanosheets do not aggregate to form the thin film.

Fig. 2d inset (up) shows a clear lattice fringe in HRTEM image. The lattice fringe spacing is measured to be 0.41 nm, according with the (111) planes of the mushroom-like Ni_3S_2. The corresponding Fast Fourier Transform (FFT) pattern also confirms the lattice fringe spacing about 0.41 nm in the HRTEM image, after the diffraction spots is calculated from the Fig. 2d inset (down).

Base on the analysis of the SEM and TEM images for different reaction time, the synthetic procedure of the mushroom-like Ni_3S_2 is schematically illustrated in Fig. 3. The nanorods Ni_3S_2 arrays were obtained after 12 h. The large number of nanosheets coating on nanorods Ni_3S_2 were prepared after 24 h in the hydrothermal reaction. After reaction time of 24 h, more and more Ni_3S_2 nanosheets were produced and aggregated to form the thin film on the top of nanorods Ni_3S_2 arrays. This phenomenon can be attributed to numerous nanosheets increasing high specific surface energy of the electrode materials. The high specific surface energy leads to nanostructure instability and promotes the nanosheets aggregating.

In the X-ray diffraction (XRD) patterns of Ni_3S_2 with the three different morphologies (Fig. 4), the well-defined diffraction peaks observed at 2θ values of 21.75, 31.1, 37.78, 49.73 and 55.16^o can be indexed to (101), (110), (003), (113) and (122) plane reflections of Ni_3S_2 phase (JCPDS-44-1418).

Fig. 5a shows the typical cyclic voltammogram (CV) curves of the mushroom-like Ni_3S_2 electrode at different scan rates of 2, 5, 7, 10, 15, 20 mV s^{-1} and the potential ranges are from 0 to 0.7 V. All of the CV curves show a visible pair of redox peaks derived from Faradaic reactions, which demonstrate the pseudocapacitive properties of the mushroom-like

CrystEngComm Accepted Manuscript

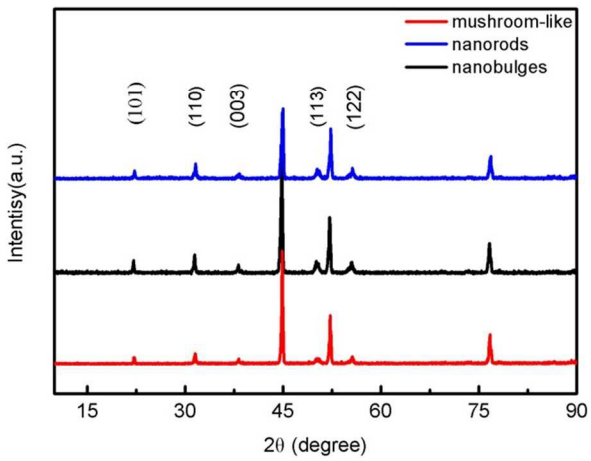

Fig. 4 XRD patterns of difference morphologies Ni_3S_2.

Ni_3S_2 electrode. The anodic peaks shifted towards positive potential and the cathodic peaks shifted towards negative potential, because the internal diffusion resistance increases with scan rate.[45-47] In Fig. 5a inset, it is concluded that the electrodes have a good quasi-reversible pseudocapacitive behavior, because the currents are nearly linearly relationship to the square root of the scan rate.[48]

Fig. 5b shows the CV curves of nanorods Ni_3S_2 arrays and mushroom-like-Ni_3S_2 electrodes at a scan rate of 5 mV s^{-1}. Obviously, the CV curve area of the mushroom-like Ni_3S_2 is larger than nanorods Ni_3S_2 arrays electrode, indicating the mushroom-like Ni_3S_2 exhibits higher electrochemistry active.[29] Galvanostatic charge–discharge measurement (GCD) demonstrates that the electrochemistry perfomance of mushroom-like Ni_3S_2 is better than nanorods Ni_3S_2 electrode, again.

The performance of GCD is a critical parameter for assessing their potential application. Fig. 5c shows the discharge curves of the mushroom-like Ni_3S_2 and nanorods Ni_3S_2 arrays electrodes at different current densities within a potential window of 0-0.5 V. The specific capacitance of the electroactive materials was calculated by equation (3).

$$C_{sp} = I \times t / \Delta V \times m \quad (3)$$

Where I is current (A), t is a full discharge time(s), V represents the total potential deviation (V), and m indicates the mass of the electroactive materials. When the discharge current densities are 1, 2, 4 and 8 F g^{-1} (Fig. 5c), the specific capacitance values of the mushroom-like Ni_3S_2 electrode are 1670, 1494.8, 1320.8 and 1190.4 F g^{-1}, respectively. With the discharge current densities increasing, the pseudocapacitance specific capacitance decreases, because the IR drop increase and electroactive materials insufficiently take part in redox reaction.[49] Fig. 5d demonstrates that the discharge time of the mushroom-like Ni_3S_2 electrode is longer than nanorods Ni_3S_2 arrays at the current density of 2 A g^{-1}. From anther figure of the charge-discharge measurement (Fig. S1), the specific capacitance values of the nanorods Ni_3S_2 arrays electrode are 1220, 922, 738.4 and 532.8 F g^{-1} at the current densities of 1, 2, 4 and 8 A g^{-1},

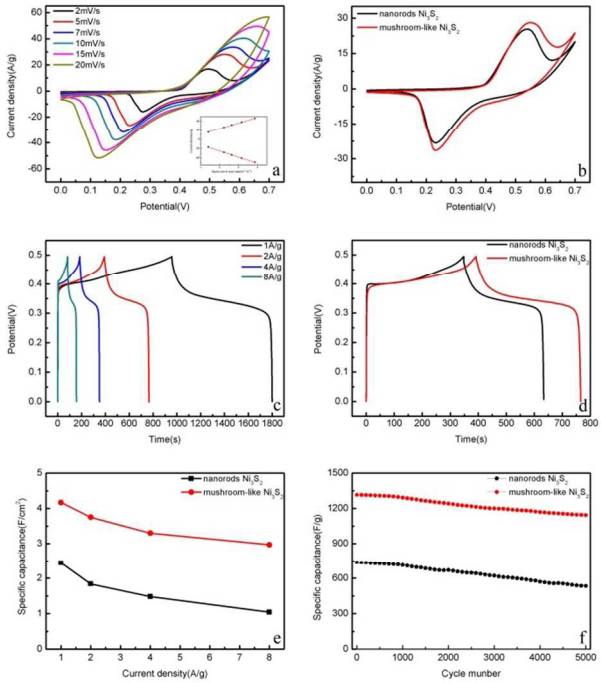

Fig. 5 (a) CV curves of mushroom-like Ni_3S_2 at different scan rate, (inset is anodic/cathodic peak currents as a function of the square root of the potential scan rate.) (b) CV curves of mushroom-like and nanorods Ni_3S_2 at a scan rate of 5 mV.s^{-1} (c) charge-discharge curves of mushroom-like Ni_3S_2 at different current densities (d) charge-discharge curves of mushroom-like and nanorods Ni_3S_2 at current density of 2 A.g^{-1} (e) the area specific capacitance of mushroom-like and nanorods Ni_3S_2 as a function of current density plot (f) cycling performance of mushroom-like and nanorods Ni_3S_2 electrode at current of 4 A g^{-1}.

respectively. Compared with the nanorods Ni_3S_2 arrays electrode, the mushroom-like Ni_3S_2 exhibits much higher specific capacitance, because the thin film provide the rich accessible electroactive sites and superior electron collection efficiency.[29] From the Fig. 5e, the area specific capacitance is calculated by equation (4):

$$C = I \times t / \Delta V \quad (4)$$

It reveals that the area specific capacitances (C) of the mushroom-like Ni_3S_2 electrode are 4.17, 3.75, 3.30 and 2.97 F cm^{-2}, and the nanorods Ni_3S_2 arrays are 2.44, 1.84, 1.48 and 1.04 F cm^{-2} at different current densities, respectively. However, C only remained 71.2% of the initial capacitance at current density of 8 A g^{-1} for the mushroom-like Ni_3S_2 electrode, but the nanorods Ni_3S_2 remained 43.4% at the same condition. The reason is the rate of alkali ions adsorption and desorption into and out of electrode materials surface controls the discharge time.[50,51] Compared with the nanorods Ni_3S_2 arrays electrode, the thin film decreases the ion adsorption and desorption rate of change with increasing the current density, resulting in thin film reduces the loss of the area specific capacitance for the mushroom-like Ni_3S_2 electrode.

The cycle of galvanostatic charge–discharge is a great important performance in practical application. As shown in Fig. 5f, the long-term cycle stability was investigated by repeating galvanostatic charge-discharge measurement at a current

CrystEngComm Accepted Manuscript

This journal is © The Royal Society of Chemistry 2012

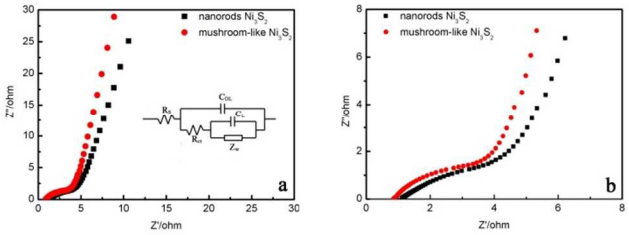

Fig. 6 EIS of the nanorods and mushroom-like Ni_3S_2 electrodes.

density of 4 A g^{-1} in the potential range of 0-0.5 V for 5000 cycles. It shows that the specific capacitance of the mushroom-like Ni_3S_2 electrode is 1316 F g^{-1} in the first cycle, after 5000 cycles it gradually decreased to 1144 F g^{-1} and retained of 86.9% overall capacitance. At the same condition, the specific capacitance of nanorods Ni_3S_2 arrays electrode is 738 F g^{-1} in the first cycle and 533.6 F g^{-1} over 5000 cycles, which retained 72.3% overall capacitance. From the both sets of data, the long-term cycle stability of the mushroom-like Ni_3S_2 electrode is better than the nanorods Ni_3S_2. Because the thin film decreases the capacitance fading of rate and protects the nanomaterial structure in a long time cycle (Fig. S2).[29]

To investigate the electrochemistry performance of the mushroom-like Ni_3S_2 and nanorods Ni_3S_2 arrays electrodes further, EIS was measured at open circuit potential in a frequency ranging from 0.01 Hz to 100 kHz. The Nyquist plots of each electrode (Fig. 6) is made up of two parts: one is a linear part which represents the Warburg impedance (Z_w) at low frequency, the other is a similar form with a semicircle which represents the charge transfer resistance (R_{ct}) in the high-frequency region. To analyze further the measured impedance spectra, the complex nonlinear least-squares (CNLS) fitting method based on the equivalent circuit (Fig. 6) is used. The fitting results are presented in Table S1. In the equivalent circuit, the R_S is bulk resistance of the electrochemical system (the intersection of the curve at real part Z' in the high frequencies range). Among all the evaluation parameters, R_{ct} of the nanorods Ni_3S_2 arrays electrode is larger than mushroom-like Ni_3S_2, indicating that the mushroom-like Ni_3S_2 electrode exhibits a higher the rate of charge diffusion than nanorods Ni_3S_2 arrays.[11,52-54] Z_w and R_S of the mushroom-like Ni_3S_2 electrode are smaller than the curve of nanorods Ni_3S_2 arrays, indicating that the mushroom-like Ni_3S_2 electrode exhibits lower diffusion resistance and bulk resistance than nanorods Ni_3S_2 arrays. This phenomenon is attributed to the mushroom-like structure that the thin film improves the utilization rate of material surface and ion diffusion efficiency. It demonstrates that the thin film accelerates the electron transfer from the surface of the electroactive materials to conductivity substrates.

From the electrochemistry measurement of three-electrode system, we conclude that the thin film plays a key role in enhancing the electrochemistry performance of the mushroom-like Ni_3S_2 electrode. Therefore, it shows several advantages to apply to supercapacitors: (1) the mushroom-like Ni_3S_2 was synthesized *via* a simple one-step method: dissolution-

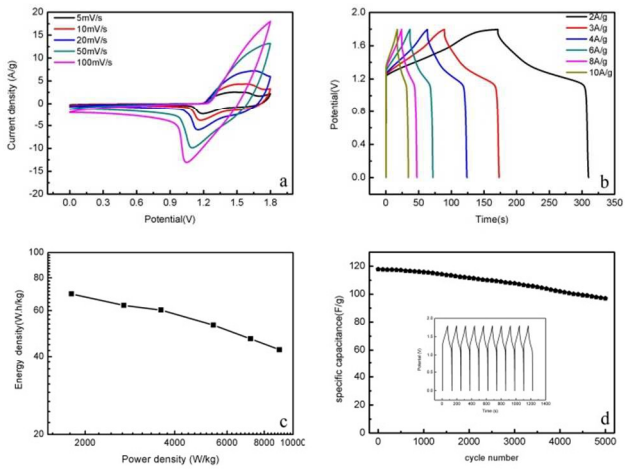

Fig. 7 (a) CV curves of mushroom-like Ni_3S_2//AC device (b) charge-discharge curves of mushroom-like Ni_3S_2//AC device at different current densities (c) Ragone pole of the mushroom-like Ni_3S_2//AC device (d) cycling performance of the mushroom-like Ni_3S_2//AC device at current density of 4 A g^{-1} (inset shows the charge-discharge curves of the first 10 cycles).

precipitation process. And the reaction time is applied to control the different morphologies: nanorods Ni_3S_2 arrays or mushroom-like Ni_3S_2. (2) For the mushroom-like Ni_3S_2 electrode, the thin film on the top of nanorods arrays improves the specific surface area and provides more active sites for absorption ions, exhibits an excellent electrochemical capacitance, high rate performance and high areal capacitance. (3) The thin film protects the nanostructure in a long time charge-discharge cycles and improves the cycle stability of the electrode materials.

To further investigate the electrochemsitry performance of the mushroom-like Ni_3S_2 electrode for practical application, the asymmetric supercapacitor device (Fig. S3) was successfully prepared. We also measured the electrochemistry performance of the negative materials (AC). Fig. S4a gives the excellent electric double layer capacitance property from the CV curves at different scan rate. From the charge-discharge curves (Fig. S4b), the specific capacitance of AC is 201.6 F g^{-1} at current density of 0.24 A g^{-1}. And the specific capacitance of the mushroom-like Ni_3S_2 is 1670 F g^{-1} at current density of 1 A g^{-1}. Therefore, it is concluded that the mass ratio of the positive and negative electrode is 0.25 from the equation (2). But in the practical measurement, the quality ratio is 0.2, because the excess AC makes better use of positive electrode materials in electrochemistry measure.

Fig. 7a shows the CV curves of the asymmetric supercapacitor from 5 to 100 mV s^{-1}. It exhibits the electrical double layer capacitor properties and pseudocapacitance capacitor properties at 0 - 1.8 V. Increasing the scan rate, a pair of oxidation and reduction peak shifts and the current of peak becomes larger and larger. Fig. 7b exhibits the GCD measurement at different current densities in potential window of 0-1.8V. It demonstrates an excellent electrochemistry reversibility because the charge curves are symmetry of the corresponding

CrystEngComm Accepted Manuscript

discharge counterparts. The specific capacitances were calculated to be 154.4, 139.34, 134, 117.34, 104, 94.4 F g^{-1}at the current densities of 2, 3, 4, 6, 8 and 10 A g^{-1}, respectively. According to the equation (5):

$$P=\frac{E}{t} \quad (5)$$

the energy of the asymmetric supercapacitor reaches 69.48 W h kg^{-1} at a power density of 1800 W kg^{-1} and still remains 42.48 W h kg^{-1} at a power density of 9000 W kg^{-1}(Fig. 7c). Compared with the reported asymmetric supercapacitors previously, the mushroom-like Ni_3S_2//AC exhibits not only a superior energy density but also power density.[11,43,55-56] This is attributed to the multidimensional and hierarchical nanostructure which can solve the serious problem that the single nanostructure electrode materials have a fast fading of capacitance for the multidimensional and hierarchical electrode materials. Compared with single nanostructure electrode materials, the mushroom-like Ni_3S_2 which is a multidimensional and hierarchical nanostructure presented rich accessible electroactive sites and superior electron collection efficiency at the electrochemistry performance measurement. [57] The GCD measurement is used to evaluate the long-term cycling stability of the as-obtained asymmetric supercapacitor in Fig. 7d. It demonstrates that the specific capacitance is still 117.4 F g^{-1} in the first cycle, after 5000 cycles, the specific capacitance decreases to 94.2 F g^{-1}. The specific capacitance remains 80.2% of the initial capacitance at the current density of 4 A g^{-1} after 5000 cycles. Fig. 7d inset demonstrates that almost the same sharp in the first 20 cycles, indicating an excellent long-term cycles stability of the asymmetric supercapacitor.

Conclusions

The mushroom-like Ni_3S_2 supported on the 3D macro-porous Ni foam was successfully fabricated by a simple dissolution-precipitation route in which Ni foam is putting into the Teflon autoclave with a homogeneous solution of TAA and ethanol. Due to the hierarchical structure, the mushroom-like Ni_3S_2 electrode with three-electrode electrochemistry measurement presented a high specific capacitance (1320.8 F g^{-1} at 4 A g^{-1}) and excellent cycling stability of charge-discharge measurement (retaining 86.9% of overall capacitance after 1000 cycles). The mushroom-like Ni_3S_2 asymmetric supercapacitor was fabricated in practical application and exhibited high energy density (60.3W h kg^{-1} at 3600 W kg^{-1}) and cycling stability (retaining 80.2% of overall capacitance after 5000 cycles at current density of 4 A g^{-1}).

Acknowledgements

This work was supported by National Natural Science Foundation of China (51402065), Heilongjiang Province Natural Science Funds for Distinguished Young Scholar (JC201404), Special Innovation Talents of Harbin Science and Technology for Distinguished Young Scholar (2014RFYXJ005), Fundamental Research Funds of the Central University (HEUCFZ), Natural Science Foundation of Heilongjiang Province（B201404）, Program of International S&T Cooperation special project (2013DFR50060), Special Innovation Talents of Harbin Science and Technology (2013RFQXJ145), and the fund for Transformation of Scientific and Technological Achievements of Harbin (2013DB4BG011), Natural Science Foundation of Heilongjiang Province (E201329), Innovation Talents of Harbin Science and Technology (2014RFQXJ035).

[a] *Key Laboratory of Superlight Material and Surface Technology, Ministry of Education, Harbin Engineering University, 150001, P. R. China.*
[b] *Institute of Advanced Marine Materials, Harbin Engineering University, 150001, P. R. China.*
** Corresponding author: Tel: +86 451 8253 3026; Fax: +86 451 8253 3026. E-mail address: zhqw1888@sohu.com.cn*

Notes and references

1. B. E. Conway, Electrochemical Supercapacitors: Scientific Fundamentals and Technological Applications, Kulwer Academic, 1999.
2. Z. Gao, J. Wang, Z. S. Li, W. L. Yang, B. Wang, M. J. Hou, Y. He, Q. Liu, T. Mann, P. P. Yang, M. L. Zhang and L. H. Liu, *Chem Mater.*, 2011, 23, 3509-3516.
3. G. H. Yu, X. Xie, L. J. Pan, Z. N. Bao and Y. Cui, *Nano Energy*, 2013, 2, 213-234.
4. H. Chen, L. F. Hu, Y. Yan, R. C. Che, M. Chen and L. M. Wu, *Adv. Energy Mater.*, 2013, 3, 1636-1646.
5. J. Yan, Z. J. Fan, W. Sun, G. Q. Ning, T. Wei, Q. Zhang, R. F. Zhang, L. J. Zhi and F. Wei, *Adv. Funct. Mater.*, 2012, 22, 2632-2641.
6. K. B. Xu, W. Y. Li, Q. Liu, B. Li, X. J. Liu, L. An, Z. G. Chen, R. J. Zou and J. Q. Hu, *J. Mater. Chem. A*, 2014, 2, 4795.
7. L. Demarconnay, E. Raymundo-Pinero and F. Beguin, *J. Power Sources*, 2011, 196, 580-586.
8. Z. S. Wu, W. C. Ren, D. W. Wang, F. Li, B. L. Liu and H. M. Cheng, *ACS Nano*, 2010, 4, 5835-5842.
9. D. W. Wang, H. T. Fang, F. Li, Z. G. Chen, Q. S. Zhong, G. Q. Lu and H. M. Cheng, *Adv. Funct. Mater.*, 2008, 18, 3787-3793.
10. L. G. H. Staaf, P. Lundgren and P. Enoksson, *Nano Energy*, 2014, 9, 128-141.
11. X. Zhang, Y. Zhao and C. Xu, *Nanoscale*, 2014, 6, 3638-3646.
12. B. Wang, Q. Liu, J. Han, X. F. Zhang, J. Wang, Z. S. Li, H. J. Yan and L. H. Liu, *J. Mater. Chem. A*, 2014, 2, 1137.
13. F. Y. Ning, M. F. Shao, C. L. Zhang, S. M. Xu, M. Wei and X. Duan, *Nano Energy*, 2014, 7, 134-142.
14. X. Wang, B. Liu, R. Liu, Q. Wang, X. Hou, D. Chen, R. Wang and G. Shen, *Angew. Chem. Int. Ed*, 2014, 53,1849-1853.
15. L. Yu, N. N. Shi, Q. Liu, J. Wang, B. Yang, B. Wang, H. J. Yan, Y. B. Sun and X. Y. Jing, *Phy. Chem. Chem. Phy.*, 2014, 16, 17936-17942.
16. H. L. Wang, H. S. Casalongue, Y. Y. Liang and H. J. Dai, *J. Am. Chem. Soc.*, 2010, 132, 7472-7477.
17. G. Q. Zhang and X. W. Lou, *Adv. Mater.*, 2013, 25, 976-979.
18. G. Q. Zhang, H. B. Wu, H. E. Hoster, M. B. Chan-Park and X. W. D. Lou, *Energy Environ. Sci.*, 2012, 5, 9453-9456.
19. Z. Y. Qian, T. Peng, J. Wang and L. T. Qu, *ChemSusChem*, 2014.
20. J. Jiang, Y. Li, J. Liu, X. Huang, C. Yuan and X. W. Lou, *Adv. Mater.*,

CrystEngComm Accepted Manuscript

 This journal is © The Royal Society of Chemistry 2012

2012, 24, 5166-5180.
21. G. P. Wang, L. Zhang and J. J. Zhang, *Chem Soc Rev*, 2012, 41, 797-828.
22. C. Z. Yuan, L. Yang, L. R. Hou, J. Y. Li, Y. X. Sun, X. G. Zhang, L. F. Shen, X. J. Lu, S. L. Xiong and X. W. Lou, *Adv. Funct. Mater.*, 2012, 22, 2560-2566.
23. D. P. Cai, B. Liu, D. D. Wang, L. L. Wang, Y. Liu, H. Li, Y. R. Wang, Q. H. Li and T. H. Wang, *J. Mater. Chem. A*, 2014, 2, 4954.
24. J. Jiang, Y. Y. Li, J. P. Liu and X. T. Huang, *Nanoscale*, 2011, 3, 45-58.
25. Y. G. Li, B. Tan and Y. Y. Wu, *Nano Lett.*, 2008, 8, 265-270.
26. D. Chao, X. Xia, C. Zhu, J. Wang, J. Liu, J. Lin, Z. Shen and H. J. Fan, *Nanoscale*, 2014, 6, 5691-5697.
27. X. H. Xia, J. P. Tu, Y. Q. Zhang, X. L. Wang, C. D. Gu, X.-b. Zhao and H. J. Fan, *ACS nano*, 2012, 6, 5531-5538.
28. T. Y. Wei, C. H. Chen, H. C. Chien, S. Y. Lu and C. C. Hu, *Adv. Mater.*, 2010, 22, 347-351.
29. L. Mei, T. Yang, C. Xu, M. Zhang, L. B. Chen, Q. H. Li and T. H. Wang, *Nano Energy*, 2014, 3, 36-45.
30. G. H. Zhang, T. H. Wang, X. Z. Yu, H. N. Zhang, H. G. Duan and B. A. Lu, *Nano Energy*, 2013, 2, 586-594.
31. X. H. Xia, C. R. Zhu, J. S. Luo, Z. Y. Zeng, C. Guan, C. F. Ng, H. Zhang and H. J. Fan, *Small*, 2014, 10, 766-773.
32. C. W. Su, J. M. Li, W. Yang and J. M. Guo, *J. Phys. Chem. C*, 2013, 118, 767-773.
33. W. J. Zhou, X. H. Cao, Z. Y. Zeng, W. H. Shi, Y. Y. Zhu, Q. Y. Yan, H. Liu, J. Y. Wang and H. Zhang, *Energy Environ. Sci.*, 2013, 6, 2216-2221.
34. Z. C. Xing, Q. X. Chu, X. B. Ren, C. J. Ge, A. H. Qusti, A. M. Asiri, A. O. Al-Youbi and X. P. Sun, *J. Power Sources*, 2014, 245, 463-467.
35. W. J. Zhou, X. J. Wu, X. H. Cao, X. Huang, C. L. Tan, J. Tian, H. Liu, J. Y. Wang and H. Zhang, *Energy Environ. Sci*, 2013, 6, 2921-2924.
36. K. Krishnamoorthy, G. K. Veerasubramani, S. Radhakrishnan and S. J. Kim, *Chem. Eng. J.*, 2014, 251, 116-122.
37. Z. Zhang, Z. Huang, L. Ren, Y. Shen, X. Qi and J. Zhong, *Electrochim. Acta*, 2014, 149, 316-323.
38. H. Huo, Y. Zhao and C. Xu, *J. Mater. Chem. A*, 2014, 2, 15111.
39. J. Xiao, L. Wan, S. H. Yang, F. Xiao and S. Wang, *Nano Lett.*, 2014, 14, 831-838.
40. Y. Zhang, M. Ma, J. Yang, C. Sun, H. Su, W. Huang and X. Dong, *Nanoscale*, 2014, 6, 9824-9830.
41. J. Q. Yang, X. C. Duan, Q. Qin and W. J. Zheng, *J. Mater. Chem. A*, 2013, 1, 7880-7884.
42. C. S. Dai, P. Y. Chien, J. Y. Lin, S. W. Chou, W. K. Wu, P. H. Li, K. Y. Wu and T. W. Lin, *ACS Appl.Mater.Inter.*, 2013, 5, 12168-12174.
43. H. C. Chen, J. J. Jiang, L. Zhang, D. D. Xia, Y. D. Zhao, D. Q. Guo, T. Qi and H. Z. Wan, *J. Power Sources*, 2014, 254, 249-257.
44. G. Q. Zhang and X. W. Lou, *Scientific reports*, 2013, 3.
45. J. Y. Ji, L. L. Zhang, H. X. Ji, Y. Li, X. Zhao, X. Bai, X. B. Fan, F. B. Zhang and R. S. Ruoff, *ACS nano*, 2013, 7, 6237-6243.
46. U. Patil, K. Gurav, V. Fulari, C. Lokhande and O. S. Joo, *J.Power Sources*, 2009, 188, 338-342.
47. Q. D. Wu, X. P. Gao, G. R. Li, G. L. Pan, T. Y. Yan and H. Y. Zhu, *J. Phys. Chem. C*, 2007, 111, 17082-17087.
48. B. Wang, Q. Liu, Z. Y. Qian, X. F. Zhang, J. Wang, Z. S. Li, H. J. Yan, Z. Gao, F. B. Zhao and L. H. Liu, *J. Power Sources*, 2014, 246, 747-753.
49. H. Z. Wan, J. J. Jiang, J. W. Yu, K. Xu, L. Miao, L. Zhang, H. C. Chen and Y. J. Ruan, *CrystEngComm*, 2013, 15, 7649-7651.
50. X. Zhu, H. Dai, J. Hu, L. Ding and L. Jiang, *J. Power Sources*, 2012, 203, 243-249.
51. Y. Bai, M. Du, J. Chang, J. Sun and L. Gao, *J. Mater. Chem. A*, 2014, 2, 3834.
52. P. Han, Y. Yue, Z. Liu, W. Xu, L. Zhang, H. Xu, S. Dong and G. Cui, *Energy Environ. Sci*, 2011, 4, 4710.
53. Y.-M. Wang, D.-D. Zhao, Y.-Q. Zhao, C.-L. Xu and H.-L. Li, *RSC Advances*, 2012, 2, 1074.
54. K. Wang, J. Y. Huang and Z. X. Wei, *J. Phys. Chem. C*, 2010, 114, 8062-8067.
55. C.-S. Dai, P.-Y. Chien, J.-Y. Lin, S.-W. Chou, W.-K. Wu, P.-H. Li, K.-Y. Wu and T.-W. Lin, *ACS Appl. Mater. Inter.*, 2013, 5, 12168-12174.
56. H. C. Chen, J. J. Jiang, L. Zhang, T. Qi, D. D. Xia and H. Z. Wan, *J. Power Sources*, 2014, 248, 28-36.
57. H. H. Huo, Y. Q. Zhao and C. L. Xu, *J. Mater. Chem. A*, 2014, 2, 15111-15117.

CrystEngComm Accepted Manuscript

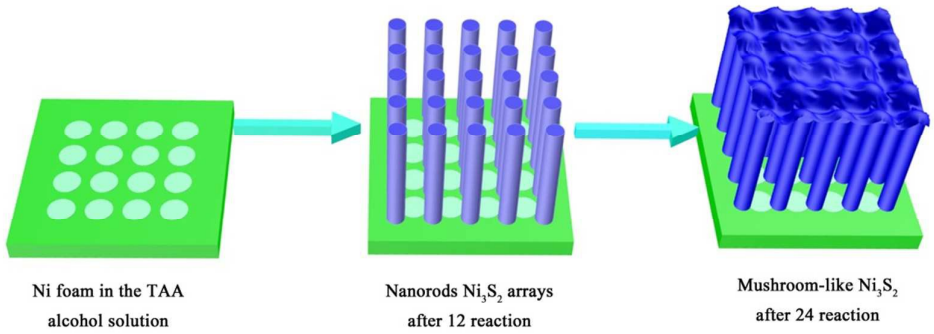

We present a simple one-step dissolution-precipitation route for the in-situ growth of the nanorods and mushroom-like Ni_3S_2 on the Ni foam (NF). It only involves a simple hydrothermal process using the NF in the thioacetamide (TAA) alcohol solution without the introduction of other Ni sources, surfactant and template. Compared with the nanorods Ni_3S_2 arrays electrode, the mushroom-like Ni_3S_2 presented rich accessible electroactive sites and superior electron collection efficiency at the electrochemistry performance measurement. The asymmetric supercapacitor, with the mushroom-like Ni_3S_2 as the positive electrode material and the active carbon powder (AC) as the negative electrode material, exhibited a high energy density (60.3 W h kg^{-1}) at an average power density of 3600 W kg^{-1} based on the mass of active material.

CrystEngComm Accepted Manuscript